Sixia Gong · Tao Zhao · Jidong Zhao · Feng Dai · Gordon G. D. Zhou

Discrete element analysis of dry granular flow impact on slit dams

Abstract Slit dam is an open-check barrier structure widely used in mountainous regions to resist the destructive impacts of granular flows. To examine the dynamics of granular flow impact on slit dams, a numerical study by discrete element method (DEM) is presented in this article. The study considers dry granular materials flowing down a flume channel and interacts with slit dams installed at the lower section of the flume. The particle shape is explicitly considered by particle clumps of various aspect ratios. The slit dams are modeled as rigid and smooth rectangular prisms uniformly spaced at in the flume. Four key stages of granular flow impact on the slit dams have been identified, namely, the frontal impact, run up, pile up, and static deposition stages. In the impact process, the kinetic energy of the granular flow is dissipated primarily by interparticle friction and damping. The trapping efficiency of the slit dams decreases exponentially with the relative post spacing, while it increases with the particle clump aspect ratio. The numerical results can provide new insights into the optimization of relative post spacing for slit dam design.

Keywords Dry granular flow · Slit dam · Discrete element method · Particle clump · Trapping efficiency

Introduction

As one of the common geological hazards, granular flow can significantly threaten human lives, structures and infrastructures, and lifeline facilities worldwide due to its fast-moving velocity, long runout distance, and high impact force (Chen et al. 2015; Hürlimann et al. 2006; Iverson 1997). Common mitigation measures are based on structural countermeasures to granular flow impacts, such as flexible barriers (Li and Zhao 2018), rigid obstacles (Teufelsbauer et al. 2011), and baffle arrays (Choi et al. 2018). As one of the most popular measures, closed check dam has the major drawback of being easily filled up by sediments due to relatively low storage capability and poor permeability (Cucchiaro et al. 2019). Failure of closed check dam may cause more devastating sediment-related secondary disasters, such as floods and debris flows. Alternative open-form barrier structures, such as slit dams and flexible barriers, have gained increasing favors in engineering practice (Choi et al. 2019; Choi et al. 2018; Zhou et al. 2019).

A slit dam usually consists of an array of densely spaced concrete columns. These columns may serve as effective measures to dissipate the impact energy of granular flow and collectively help to retain a certain portion of coarse solids (Cui et al. 2018). It can thus control the peak granular discharge by allowing a relatively small portion of debris materials to pass through the slits. This approach may significantly reduce the destructive power of granular flow and thus the possibility of dam failure (Goodwin and Choi 2020). The performance of slit dam is influenced primarily by the so-called relative post spacing (Choi et al. 2016), which is defined as the ratio of the post spacing (b) of the dam to the maximum particle diameter ($d_{\max}$) of the debris materials. Ikeya and Uehara (1980) studied the response of different open-type dams and concluded that the slit dam could be blocked when $b/d_{\max}$ is less than 1.5. Some recent field investigations also showed that slit dams with narrow relative post spacing ($b/d_{\max} \approx 1.5$) are more vulnerable to be filled up (Shima et al. 2016). Han and Ou (2006) identified three patterns of slit dam blockage by nonviscous debris flows in the field, namely, complete blockage, partial blockage, and opening. They further concluded that the complete blockage would occur for a slit dam with $b/d_{\max}$ being smaller than 1.5.

To explore the fundamental mechanisms of granular flow regulation, it is imperative to analyze the interactions between the solid materials and barrier structures, which can be conveniently investigated by the discrete element method (DEM). The DEM has been widely used to investigate the behavior of geohazards including granular flows and rock avalanches (Bonilla-Sierra et al. 2015; Choi et al. 2014; Li and Zhao 2018). Choi et al. (2014) performed both physical model tests and DEM simulations on debris flow mitigation measures to examine the key interaction mechanisms between baffle arrays and debris flows. They concluded that the baffle spacing should be 0.25 times of the channel width for the optimized mitigating performance. Law et al. (2015) employed DEM simulations to study the granular flow impact with various baffle configurations. They proposed the optimum baffle spacing based on the minimized peak impact force acting on the rigid barrier. In the field, the debris particles are commonly angular in shape which may affect the particle-particle interactions, particle-bed interactions, and particle-barrier interactions and thus underpin its overall mobility, impact, and deposition (Dong et al. 2015). It is thus critically important to consider the particle shape effect in DEM simulations (Ferellec and McDowell 2010).

This study aims to investigate the influence of particle shape on the dynamics of granular flow and its impact on slit dams by DEM to offer new insights in practical engineering designs. The numerical model employs clumped particles to represent irregularly shaped particles. Since the shape of constituent particles remains spherical, the contact detections and interparticle force calculations can still follow those used in conventional DEM simulations. The article is organized as follows: section 2 presents a brief introduction to the DEM model configurations. In Section 3, the obtained numerical results are illustrated. Section 4 provides discussions on model size and granular flow inertia effects on modeling granular flow impact. Finally, the conclusions reached in this study are summarized in Section 5.

Methodology and model configurations

The open-source DEM code ESyS-Particle (Weatherley et al. 2011) has been employed in this study to run all the simulations presented herein. In the DEM model, the dynamics of each

individual particle are governed by Newton's second law of motion as:

$$F_i = m_i \frac{d^2}{dt^2} r_i \tag{1}$$

$$M_i = I_i \frac{d\omega_i}{dt} \tag{2}$$

where F_i is the total force acting on particle i; r_i is the position of particle centroid; m_i is the particle mass; M_i is the total moment acting on the particle; ω_i is the angular velocity; and I_i is the moment of inertia.

Particle clump model

The particle shape in DEM is explicitly approximated by clumped particles, as shown in Fig. 1. In this model, two spherical particles are firmly bonded together via the parallel bond model (PBM) (Wang 2009) to form an unbreakable particle clump. The bonding forces between particles are calculated as follows:

$$F_{bn} = K_{bn} \cdot \Delta u_n \tag{3}$$

$$F_{bs} = K_{bs} \cdot \Delta u_s \tag{4}$$

$$M_b = K_b \cdot \Delta\theta_b \qquad M_t = K_t \cdot \Delta\theta_t \tag{5}$$

where F_{bn} and F_{bs} are the normal and shear bonding forces; M_b and M_t are the bending and twisting moments, respectively; u_n, u_s, θ_b, and θ_t are the relative displacements between the bonded particles in the normal, shear, bending, and twisting directions, respectively; K_{bn}, K_{bs}, K_b, and K_t are the corresponding bonding stiffness in the respective directions. The relative displacements are computed by unit quaternions for 3D spatial rotations of the two rigid spheres (Hamilton 1844). In this study, the bonding strength is set to be an extremely high value, e.g., 10^{20} Pa, so that the structure of clumped particles can resist any external loading without breakage.

In order to maintain the same debris mass for different tests, the density of individual particles in the clump is scaled up with respect to the clump volume, so that the bulk density of the particle clump can match that of a spherical particle. In this approach, the initial total granular energy can maintain consistently the same for all tests. The non-sphericity of particle clump is quantified by clump aspect ratio, α, defined as the ratio of the maximum distance from the clump edge (dotted line) to the geometric center (l) to the radius of individual sphere (r) (see Fig. 1). As stated by Guises et al. (2009), this definition can approximately capture the difference between various non-spherical particles for an intuitive and convenient representation.

In this research, three sets of particle shape configurations have been used, with $\alpha = 1$, 1.5, and 2, denoted as "A-1," "A-2," and "A-3," respectively. In addition, an additional series of simulations "A-4" using a mixture of equal number of particle clumps "A-1," "A-2," and "A-3" is also included for comparison purpose.

Linear elastic contact model

The interactions between individual particle clumps are computed via the linear elastic contact law in conjunction with the Coulomb friction model. In the model, the normal contact force is calculated as:

$$F_n = K_n U_n + F_n^d \tag{6}$$

where U_n is the overlapping distance in the normal direction between the two particles in contact and $K_n = \pi E \overline{R}/2$ is the normal contact stiffness, with E and $\overline{R}$ being the particle Young's modulus and mean radius. $F_n^d = -2\beta\sqrt{0.5(m_A + m_B)K_n}v_n$ is the normal damping force, where β is the damping coefficient; m_A and m_B are the masses of the two particles; v_n is the relative velocity between the two particles. In the simulations, a small damping coefficient of $\beta = 0.01$ is applied at particle contacts to account for the energy dissipation by plastic deformations. The damping coefficient is determined by trial and error to ensure it has negligible influence on the overall dynamics of granular flow. The choice is in line with the DEM model configurations in Zhao et al. (2017).

The tangential contact force is calculated incrementally as follows:

$$F_t^n = F_t^{n-1} + K_s \cdot \Delta U_t \tag{7}$$

where F_t^n and F_t^{n-1} are the tangential forces calculated at the current and previous iteration steps; $K_s = \pi E \overline{R}/(4(1 + \upsilon))$ is the shear stiffness, with E and υ being the particle Young's modulus and Poisson ratio, respectively; U_t is the incremental tangential sliding displacement. The maximum tangential force is limited by the Mohr–Coulomb criterion (Utili et al. 2015).

Model calibration

The proposed DEM model has been calibrated by performing the simulations of the collapse of a granular column and comparing the numerical results with the well-documented experimental and numerical data in the literature. The investigation of granular column collapse has been recognized as one of the most important approaches for studying the transient granular flow conditions (Crosta et al. 2009). The test involves the collapse of a column of densely packed granular materials with the initial length L_i and height H_i. The granular flow is triggered by quickly removing the frontal confining gate. At the end of the test, the final runout length of the granular materials is measured as L_f. The angle of repose, ϕ, is measured as the steepest angle of the descent of the final granular deposit relative to the horizontal plane, when grains on the slope surface are on the verge of sliding. The input parameters of the DEM simulations are listed in Table 1.

Figure 2 illustrates that the final runout distance of granular materials increases with the column aspect ratio but decreases
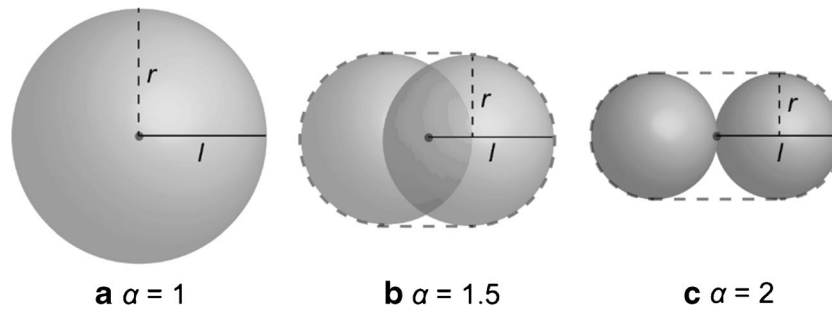
Fig. 1 Schematic view of particle clumps of different aspect ratios ($\alpha = l/r$): (a) spherical particle ($\alpha = 1$); (b) elliptical particle clump ($\alpha = 1.5$); (c) elongated particle clump ($\alpha = 2$). The dashed curve represents the approximated real particle shape

with the increase of particle clump aspect ratio in the numerical study. Granular columns consisting of spherical particles ($\alpha = 1$) have much higher spreading mobility than those of non-spherical particles, indicating that the traditional DEM model using only spherical particles would significantly overestimate the dynamics of granular flow. Conversely, the simulations with particle clumps of various particle aspect ratios can effectively mimic the dynamic responses of granular flow. In particular, the numerical results of tests using the particle clumps of $\alpha = 1.5$ can match well from a qualitative viewpoint both the experimental observations in Lube et al. (2005) and the 2D FEM numerical analyses in Crosta et al. (2009). The simulations using clump mixture can match well with the numerical results of Utili et al. (2015) for 3D DEM simulations in plane strain boundary conditions. The test with $\alpha = 2.0$ produced the shortest granular runout distance due to the high non-sphericity of particle shape. The comparisons in Fig. 2 show that the proposed particle clump model and input parameters are valid in modeling the dynamics of granular flow.

In this study, the measurement of the angle of repose (ϕ) is also performed on short granular columns (aspect ratio $a = 1.0$, to avoid the influence of intense granular dynamics on the final granular deposition). The values of ϕ are 16°, 25°, 26°, and 23° for the tests with $\alpha = 1.0$, 1.5, 2.0, and clump mixture, respectively. The spherical particles ($\alpha = 1.0$) have the lowest angle of repose, indicating that the granular flow has a very high mobility. The use of particle clumps can lead to a much higher angle of repose (e.g., 7° ~ 10° more), such that realistic internal resistance (e.g., particle friction and interlocking) of granular flow can be reproduced. The obtained results can match well the data reported in Marchelli et al. (2020) with ϕ in the range of 18° to 27°, in which the particle shape effect is characterized by the DEM rolling resistance model.

The calibration focuses mainly on the dynamic properties of granular materials, e.g., the dynamic friction (particle contact friction and interlocking) and collective particle interactions, arguably the most important material behavior governing the mobility of granular flows. The impact process has been studied in one of our previous publications on granular flow-rigid barrier impact via DEM modeling (Shen et al. 2018). Thus, the calibrated DEM model can be employed to simulate the dynamics and impacting process of granular flow.

Numerical model configurations

In this study, the DEM simulation of dry granular flow impact on a slit dam is configured according to the experiments performed by Zhou et al. (2019) in analyzing a natural debris flow sloping channel in Kangding, Sichuan, China. As shown in Fig. 3(a) and (b), the numerical model consists of a storage tank, a debris propagation zone with two different inclined flumes, and a deposition zone of an outflow leveled ground. The storage tank has the dimensions of 0.8 m in length, 0.6 m in width, and 0.4 m in height. The slope angles of the upstream (θ_1) and downstream (θ_2) flumes are 30° and 7.6°, respectively. The steep and gentle flume sections are employed to mimic the transportation and deposition zones of natural debris flow channels. The granular assembly of "A-1" consists of 60,090 polydisperse spherical particles of diameters ranging from 10 to 30 mm. Debris samples of "A-2" and "A-3" are generated by replacing the spherical particles in "A-1" with the corresponding particle clumps. The diameters of individual particles in "A-2" and "A-3" clumps are in the ranges of 6.67–20 and 5–15 mm, respectively. The mixed granular assembly "A-4" is generated by randomly replacing 1/3 of "A-1" particles with "A-2" clump

Table 1 Input parameters of DEM simulations

DEM parameters	Value	DEM parameters	Value
Particle diameter, d (mm)	5–30	Particle Poisson's ratio, υ	0.25
Particle density in A-1, ρ_1 (kg/m³)	2650	Particle friction coefficient, μ_1	0.577
Particle density in A-2, ρ_2 (kg/m³)	4472	Gravitational acceleration, g (m/s²)	9.81
Particle density in A-3, ρ_3 (kg/m³)	10600	DEM time step size, t (s)	1×10^{-5}
Young's modulus of particle, E (Pa)	10^8		

The particle densities, ρ_2 and ρ_3, are scaled up so that the bulk density of the particle clump can match that of a spherical particle (ρ_1). This is to maintain the same debris mass for different tests
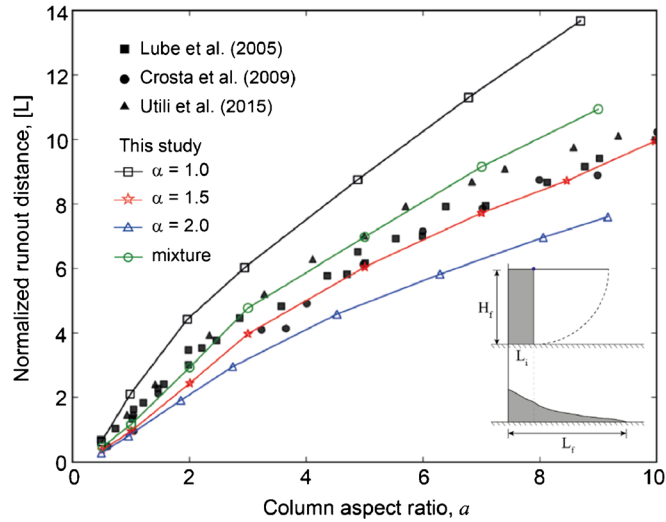
Fig. 2 Comparison of the results from numerical simulations of this study, experimental data in Lube et al. (2005), numerical data in Crosta et al. (2009), and Utili et al. (2015). Lube et al. (2005) performed the experiments using the coarse quartz sands. Crosta et al. (2009) employed finite element simulations. Utili et al. (2015) used the DEM simulations considering the particle shape effect by the rolling resistance model. All research employed the same granular column collapse setup, as shown in the inset plot. The column aspect ratio is defined as $a = H_i/L_i$, while the normalized runout distance is computed as $[L] = (L_f - L_i)/L_i$. The angle of repose, ϕ, is measured as the steepest angle of the descent of the final granular deposit relative to the horizontal plane

and another 1/3 with "A-3" clumps. The particle size distributions (PSD) employed in the simulations are illustrated in Fig. 4.

The granular particles are initially packed in the storage tank under gravity. The frontal trigger gate is then lifted rapidly to release the

granular materials to flow down the flume. The roughness of the flume base is modeled by paving a layer of spherical particles of uniform radius 10.0 mm on the bed. Since few particles can reach the horizontal outflow/deposition plane, the outflow plane is covered by a layer of
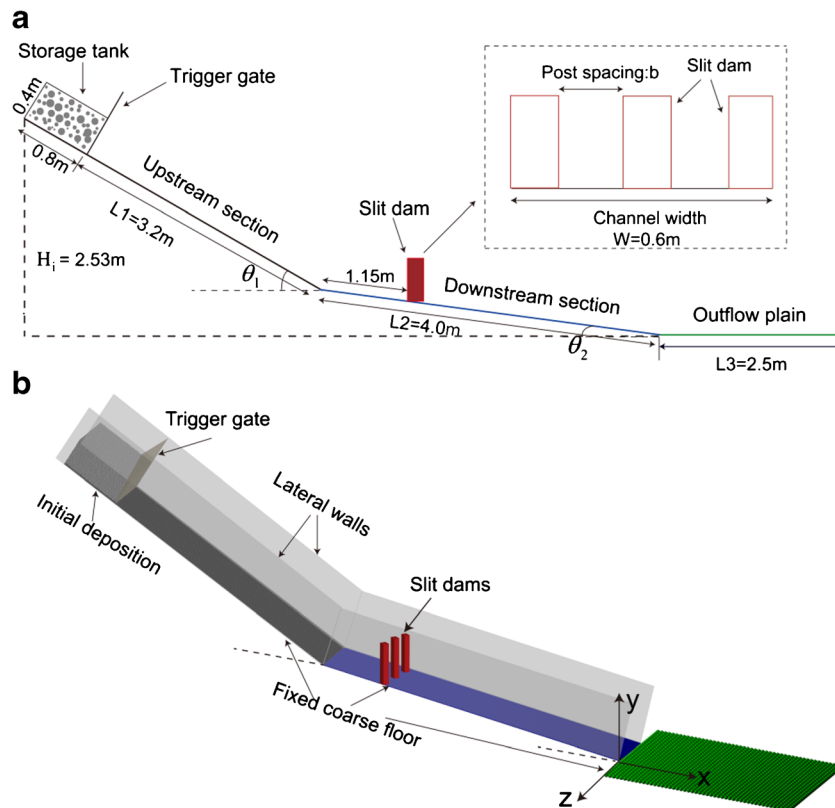

Fig. 3 (a) Configuration of the numerical model (after Zhou et al. (2019)). The inset plot shows the arrangement of slit dam. (b) A sketch of the numerical model
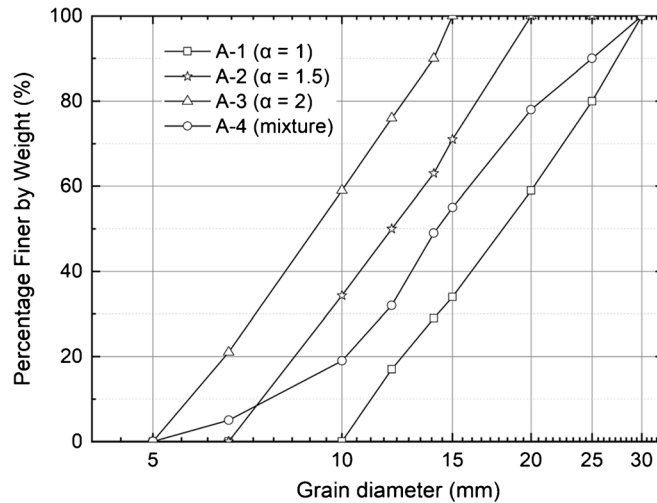
Fig. 4 Particle size distribution of granular materials with different particle aspect ratio (α) used in numerical simulations. For clumps, the grain diameter is calculated as the equivalent diameter of a sphere with the same volume as the clump

coarser particles of 25 mm in radius to increase the overall computational efficiency. For simplicity, two frictionless rigid walls are used in the lateral direction of the channel to reduce the resistance of granular dynamics from the boundary walls (Utili et al. 2015). A relatively low particle-channel friction angle of 10° is used to account for the relatively low roughness of slope surface. The slit dams are modeled as smooth rectangular prisms of a fixed height of 0.3 m with an adjustable width. They are installed at 2.85 m upstream of the channel slope toe (see Fig. 3 (a)). The location is selected such that the kinetic energy of the granular flow can be significantly reduced at the impact with the lower gentle flume before it reaches the slit dam. In this approach, the slit dam can effectively resist the impact pressure from the granular flow and at the same time discharge a good portion of particles through the slits. The width of the dam (W) is fixed as 0.6 m, while the spacing between slit posts (b) varies for different tests.

Experimental observations by Han and Ou (2006) illustrate that the slit density ($\sum b/W$) can have a significant influence on debris dynamics when it varies from 0.2 to 0.5. In the current study, five different slit densities between 0.0 and 0.7 have been employed in the simulations. The corresponding post spacing (b) and relative post spacing ratios (b/d_{max}) are listed in Table 2. Since the maximum particle diameter (d_{max}) and channel width (W) are fixed, the variations of b/d_{max} and $\sum b/W$ are caused by the change of post spacing (b). The extreme case of $b = 0$ (i.e., no slit) has also been included for comparison purpose.

Numerical results

In the analyses below, the dimensionless variables are used, such that the generality of the research outcomes can be held. In particular, the simulation time is normalized by $\sqrt{H_i/g}$, where H_i is the height of the granular flow channel (see Fig. 3a) and g is the gravitational acceleration.

Dynamics of debris-slit dam interaction

To highlight the dynamics of debris-slit dam interactions and the influence of post spacing, tests using the spherical particles (A-1, α

= 1) for two typical relative post spacings (i.e., b/d_{max} = 3 and 7) are analyzed in this section. In the analyses, for better visualization, the granular materials have been divided into five portions (i.e., P1, P2, P3, P4, and P5, with each portion contains the same number of particles) along the horizontal direction at [t] = 1.4 (the time instant just before the impact).

Figure 5 shows the lateral view of the granular flow propagation and interaction with the slit dam for the test of b/d_{max} = 3. As the granular flow front collides onto the slit dam at [t] = 2.4 (Fig. 5a), a small number of particles in P1 are discharged through the slits, while some particles are retained by the dam ([t] = 2.8, Fig. 5b). Some particles at the surface bounce back after colliding with the dam, resembling the phenomenon of "backflow" as observed in Zhou et al. (2019). With further deposition, the incoming particles have oblique shock impact with the dam and subsequently overtop the dam (see Fig. 5c). While the overtopped particles flow downstream over the channel, a certain dead zone is gradually formed at the upstream side behind the slit dam. This dead zone may serve as a cushion layer to reduce the dynamics of the incoming particles as their kinetic energy can be partially dissipated via the interparticle collision and friction with particles in the dead zone (Shen et al. 2018). With gradual piling up of particles in the dead zone (Fig. 5d and e), only about 26% of total granular mass can pass through the slits and deposits onto the downstream ground (Fig. 5f). Notably, the height of final static dead zone is slightly higher than that of the dam.

Figure 6 presents the numerical results for the simulation of b/d_{max} = 7. At [t] = 2.8 (Fig. 6b), the majority of particles in the frontal section (P1) has flowed through the slits at high speeds and only a small amount of incoming granular particles in the upstream of the slit dam start to "backflow". At [t] = 3.2 (Fig. 6c), more incoming particles can flow through the slits. Part of the granular materials bounce back from the slit dams and collide with the incoming flows to form the granular bore. These particles subsequently form a dead zone at the upstream side behind the slit dam, as captured in Fig. 6(d) and (e). The final height of the granular deposit is lower than the dam height. Compared with Fig.

Table 2 Parameters of the slit dam configuration

Channel width W (m)	Maximum diameter d_{max}	Post spacing b (m)	Relative post spacing b/d_{max}	Slit density $\Sigma b/W$
0.6	0.03	0	0	0
		0.03	1.0	0.1
		0.09	3.0	0.3
		0.15	5.0	0.5
		0.21	7.0	0.7

5, it is worth noting that as b/d_{max} increases from 3 to 7; more granular materials can pass through the slits. The evolutions of granular flow run up, pile up, and dead zone formation have also been observed in laboratory experiments (Choi et al. 2016).

Evolution of granular energy

The analysis of granular energy evolution can provide some new insights into the debris dynamics and debris-structure interactions. The total energy of the granular system consists of the potential energy (E_P), kinetic energy (E_K), the elastic energy stored at each contact between any two particles (E_s), energy loss due to local contact viscous damping (E_d), and friction (E_f).

The potential energy (E_P) at any time is defined with respect to the elevation of the outflow plain as:

$$E_p = \sum_{i=1}^{N} m_i g h_i \tag{8}$$

where N is the total number of particles in the granular system; m_i and h_i are the mass and height of particle i, respectively. Before releasing, the value of E_P is equal to the initial total energy of the granular system (E_o). In the following analyses, all energy components will be normalized by E_o.

The kinetic energy of the system at any time is calculated as:

$$E_K = \frac{1}{2} \sum_{i=1}^{N} \left(m_i |v_i|^2 + I_i |\omega_i|^2 \right) \tag{9}$$

where v_i and ω_i are the translational and angular velocities of particle i, respectively. $I_i = 2m_i r_i^2/5$ is the moment of inertia, with r_i being the particle radius.

The elastic strain energy (E_s) is the energy stored at the normal and tangential contacts, which can be calculated as:

$$E_s = \frac{1}{2} \sum_{i=1}^{N_c} \left(\frac{|F_{n,i}|^2}{K_n} + \frac{|F_{t,i}|^2}{K_s} \right) \tag{10}$$

where N_c is the total number of contacts in the granular system; $F_{n,i}$ and $F_{t,i}$ are the normal and tangential contact forces at the contact i. As mentioned in Shen et al. (2018), E_s is negligibly small in a granular flow. Thus, it is not analyzed in this study.

The energy loss due to viscous damping (E_d) at particle contacts is computed as:

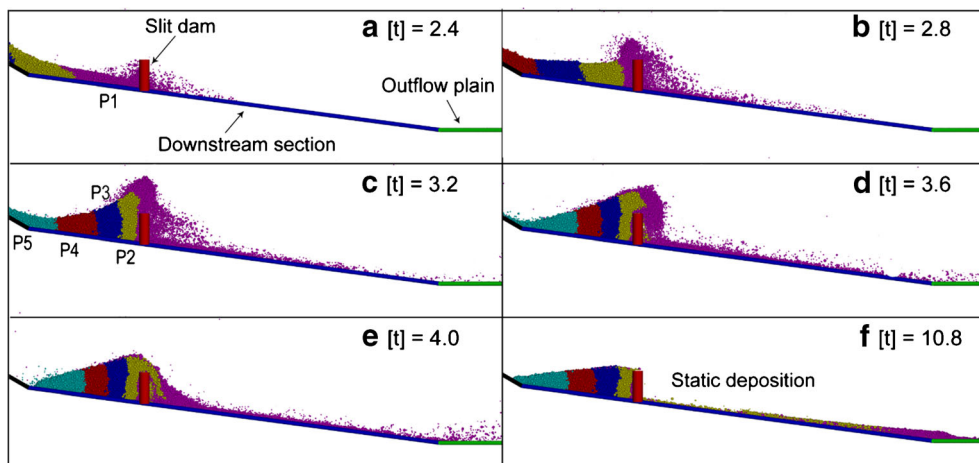$$E_d^t = E_d^{t-1} + \sum_{i=1}^{N_c} \left(F_{n,i} \Delta U_{n,i} \right) \tag{11}$$

Fig. 5 Dynamic interactions between debris flow and slit dam ($b/d_{max} = 3$, A-1 ($\alpha = 1$))
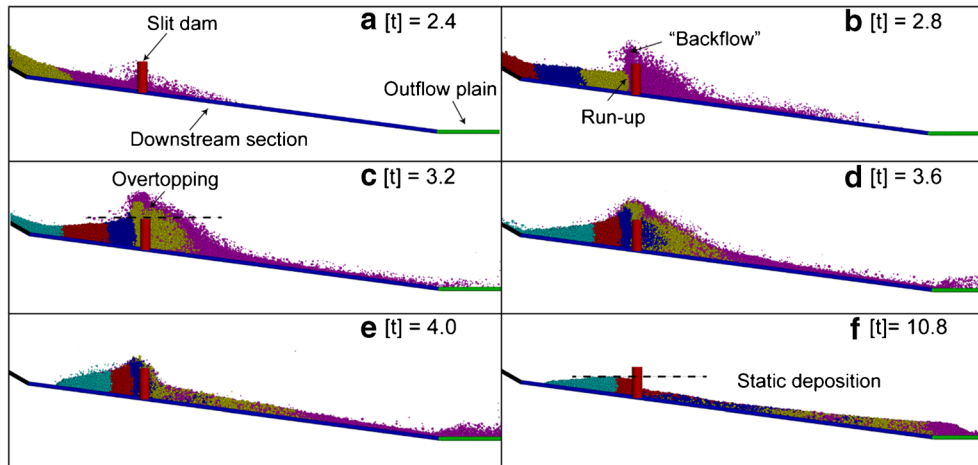
Fig. 6 Dynamic interactions between debris flow and slit dam ($b/d_{max} = 7$, A-1 ($\alpha = 1$))

where E_d^t and E_d^{t-1} are the cumulative energy loss by viscous damping at the current and previous time steps, respectively; $\Delta U_{n,\,i}$ is the increment of relative normal displacement between two particles in contact during one iteration time step. The summation is overall contacts (N_c).

Analogously, the energy loss due to friction (E_f) between any two particles can be computed as:

$$E_f^t = E_f^{t-1} + \sum_{i=1}^{N_c}\left(F_{t,i}\Delta U_{t,i}\right) \tag{12}$$

where E_f^t and E_f^{t-1} are the cumulative energy loss by friction at the current and previous time steps.

In the following analyses, the energy dissipations by damping and friction forces for particle-channel (E_d^c and E_f^c) and particle-particle (E_d^p and E_f^p) interactions will be investigated separately to quantify the relative importance of these two energy dissipation mechanisms.

Figure 7 shows the evolution of granular energy components during a simulation with $b/d_{max} = 3$, $\alpha = 1$. According to the figure, the potential energy (E_p) decreases continuously and transforms progressively into kinetic energy as the granular flow propagates downslope towards the slit dam. After the granular particles reach the dam ($[t] = 2.4$), the rate of energy dissipation increases rapidly due to intense interparticle friction and plastic collisions. The kinetic energy reaches the peak value at $[t] = 3.4$, when the rate of cumulative energy loss due to interparticle damping and friction also reach the peak values. In the final static deposition, the kinetic energy (E_K) becomes zero and the potential energy is only 17.7%. The cumulative energy losses by viscous damping (E_d^c) and friction (E_f^c) between particles and channel base are only 1.1% and 1.2%, respectively, while the cumulative energy loss due to interparticle damping (E_d^p) and friction (E_f^p) are 19.1% and 60.8%, respectively. Therefore, the energy loss during the granular flow and impact is mainly by interparticle viscous damping and friction, while the influence of particle-channel contacts (i.e., damping and friction) is negligibly small.

Trapping efficiency

Trapping or retaining the granular materials by check dams can effectively reduce the hazards posed by granular flows on infrastructures located in the downstream areas. However, high trapping efficiency may also lead the countermeasure structures to be easily filled up and lose their designed regulation function (Ng et al. 2015; Zhou and Sun 2013). Therefore, it is imperative to achieve a balanced trapping efficiency in designing slit dams. In this study, the trapping efficiency of a slit dam is defined as the ratio of the debris mass retained by the slit dam (M) to the total debris mass (M_T) (Choi et al. 2018). It is calculated when the granular flow is in the static state and the kinetic energy of the whole granular system approaches zero (see Fig. 7).

Figure 8 shows the relationship between the trapping efficiency and relative post spacing for tests using various particle shapes. The general trend shows that the trapping efficiency of a slit dam decreases exponentially with the increase of relative post spacing. The numerical data can be fitted by a general exponential function as:

$$T = a_1 e^{-a_2(b/d_{max})} + a_3 \tag{13}$$

where a_1, a_2, and a_3 are fitting coefficients.

At small relative post spacing ($b/d_{max} = 0$, 1), the majority of granular materials can be retained by the dam, resulting in high trapping efficiency in the range of 82 to 100%. This feature matches well the numerical results obtained in Marchelli et al. (2020) and experimental observations in Zhou et al. (2019). At $b/d_{max} = 0$, a small number of particles can overtop the dam in tests using A-1, A-2, and A-4, resulting in the trapping efficiency less than 100%. On the other hand, at larger relative post spacing (e.g., $b/d_{max} = 7$), a small number of particles can be retained by the slit dam, resulting in low trapping efficiency ranging from 26 to 57%. The results indicate that as b/d_{max} increases, the blockage pattern of slit dam transforms gradually from complete blockage to partial blockage or non-blockage, which matches well the observations in Han and Ou (2006). The general decreasing trend of granular trapping efficiency with the relative post spacing can
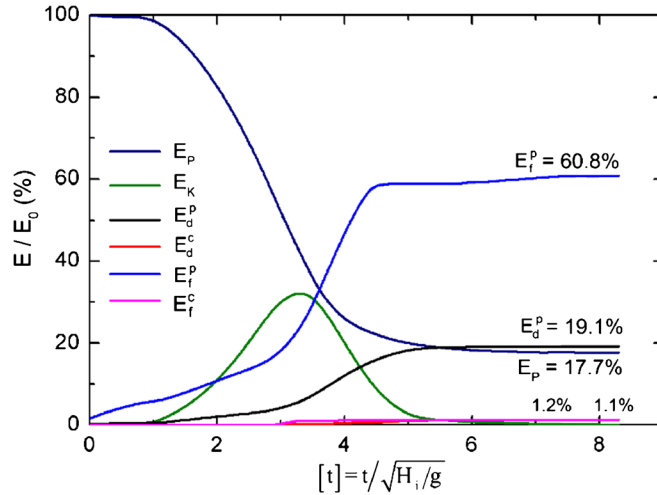
Fig. 7 Evolution of debris energy during a simulation with $b/d_{max} = 3$, A-1 ($\alpha = 1$). (E_P, potential energy; E_K, kinetic energy; E_d^c and E_f^c, energy dissipations by damping and friction for particle-channel interactions; E_f^p and E_d^p, energy dissipations by damping and friction for particle-particle interactions)

qualitatively match the results of DEM modeling by Marchelli et al. (2020) and experimental investigations by Zhou et al. (2019). In Zhou et al. (2019), the debris materials were mixed with different contents of water to mimic natural debris flow impacts on a slit dam, while in Marchelli et al. (2020), the spherical particles flowing down a steep flume were employed in the simulations. The two types of materials used in these testing configurations exhibited much higher mobilities than that of particle clumps used in this study, leading to much lower trapping efficiency.

At any specific relative post spacing, the trapping efficiency of the slit dams increases with the particle aspect ratio (α). The granular assembly composed of spherical particles (i.e., A-1 ($\alpha =$

1)) exhibits a much lower trapping efficiency when compared with those composed of sphere clumps (e.g., A-2 ($\alpha = 1.5$), A-3 ($\alpha = 2$), and A-4 (mixture)). This phenomenon is as expected as the spherical particles have a much lower apparent friction resistance (i.e., sliding and rolling) than the non-spherical particles (i.e., sliding and interlocking). The high friction of particle clumps comes from the intense particle interlocking and high rotational constraint. The tests using granular mixture exhibit an intermediate trapping efficiency because the existence of spherical particles can increase the overall mobility of granular flow. The dynamics of particle clumps can match well with the observation in Zhao et al. (2015) that the shear resistance of a granular assembly increases with the non-sphericity of the constituent particles.
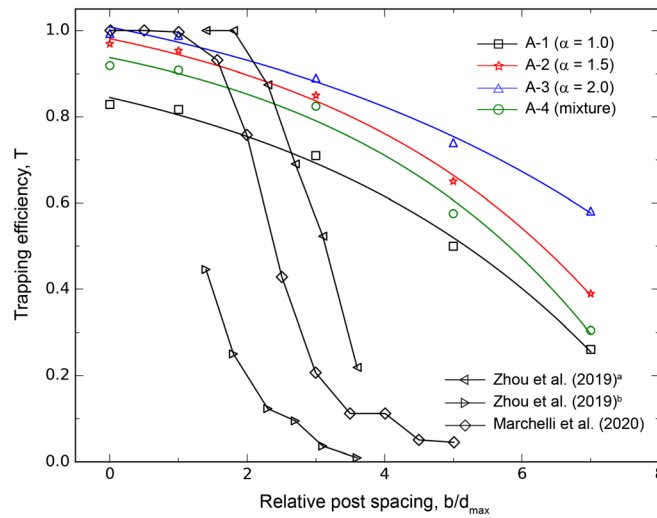

Fig. 8 Trapping efficiency of slit dam for tests of various relative post spacings (b/d_{max}) and particle clump aspect ratios. Zhou et al. (2019)[a] and Zhou et al. (2019)[b] are experimental data of debris flow impacting on slit dams with the water contents of 18% and 26%, respectively. The data of Marchelli et al. (2020) comes from the numerical simulations of granular flow by DEM using spherical particles on a steep flume (the slope angle of the flume is 30°)

Table 3 A summary of F_r and h/d for DEM simulations in this study

Test	Particle clump aspect ratio, α	Flow approaching velocity (m/s)	Flow depth (m)	Froude number, F_r	Flow depth to particle diameter ratio, h/d
A-1	1	4.48	0.123	4.1	6.15
A-2	1.5	3.46	0.081	3.9	6.07
A-3	2	3.03	0.065	3.8	6.50
A-4	Mixture	4.22	0.117	4.0	7.26

Discussion

Model size effect

As stated in Iverson (2015), a set of dimensionless parameters can be used to classify dry granular flows with various behaviors. Among others, the Froude number, F_r, and the ratio of flow depth (h) to particle diameter (d) are important parameters used in designing physical models to achieve dynamic similarity between the model and prototype (Choi et al. 2016). The Froude number is defined as the ratio of inertial to gravitational forces as $F_r = v/\sqrt{gh\cos\theta_2}$, where v is the velocity of debris front reaching the slit dams, g is the gravitational acceleration, h is the depth of flow reaching the slit dam, and θ_2 is the inclination angle of the downstream channel.

For channelized granular flow, F_r normally ranges from 0.5 to 7.6 in field observations. In some exceptional cases of water-laden debris flows, F_r can even exceed 10 (Kwan et al. 2015; McArdell et al. 2007). In this study, the Froude number of granular flow ranges from 3.8 to 4.1 as measured at the instant when the flow front approaches the slit dam (see Table 3). This value can reasonably match those observed in the field. The ratio of flow depth to particle diameter (h/d) ranges from 6.07 to 7.26, which is close to the value 7.4 reported in Choi et al. (2016) for flume test of granular flows along an inclined channel (30°). The slight difference between the numerical and experimental results may result from the larger diameter of the constituent particles used in DEM simulations. Therefore, the current numerical analyses are considered reliable for investigating the interactions between granular flow and slit dams. The numerical model in this study can be considered identical to a type of dry granular flows with F_r in the range of 3.8 to 4.1 and h/d in the range of 6.07 ~ 7.26.

Granular inertial number

Dry granular flow dissipates the kinetic energy primarily by friction and plastic collisions between individual grains. As one of the key parameters governing the granular flow dynamics, the inertial number I is defined as the ratio of mesoscopic stresses between the grain collision and frictional contacts, which can be calculated as $I = \frac{\dot{\gamma}d}{\sqrt{gh}}$, where $\dot{\gamma}$ is the shear rate of the granular flow calculated by the ratio of the flow velocity (v) to the depth (h). According to Leonardi et al. (2019), the collision stress is dominant when $I > 0.1$, namely, the corresponding granular flow regime, is regarded as a collision significant flow. While for the case of $I < 0.1$, the granular flow can be considered shearing dominant, as the shearing stress becomes much higher than the granular collision. In this study, the inertial number of tests A-1, A-2, A-3, and A-4 are 0.66, 0.64, 0.58, and 0.65, respectively. Thus, the granular flows simulated in this study are collision dominated.

Conclusions

The impacts of dry granular flows on slit dams of various post spacings have been analyzed via numerical flume tests using the open-source DEM code ESyS-Particle. The particle shape effect has been explicitly considered in the simulations by the bonded particle clump model. The obtained numerical results reveal the dynamics of debris-dam interactions, with the potential applications to a rigid slit dam design.

Based on the analyses, the non-spherical particles used in DEM simulation can effectively reproduce the dynamics of granular flows. In the process of granular flow impacting on slit dams, four essential interaction stages have been identified, namely, the frontal impact, run up, pile up, and static deposition stages. During the impact, the slit dam decelerates the granular materials to form a dead zone in the upstream behind the dam, which accumulates gradually to finally block the dam. In this process, the granular energy dissipates primarily via interparticle viscous damping and friction interactions. The trapping efficiency decreases exponentially with the increasing relative post spacing, while it increases with the particle aspect ratio (α). The trapping efficiency of the slit dams of various configuration spans a wide range, indicating that reasonable selections of relative post spacing are necessary for designing reliable slit dams with optimized regulation functions. The numerical results obtained in this research can provide some new insights into the optimization of relative post spacing for slit dam designs.

Compliance with ethical standards

Conflicts of interest   The authors declare that they have no conflict of interest.

Ethics approval   Not applicable.

Consent to participate Not applicable.

Consent for publication The authors declare that this is an original article which has neither previously, nor simultaneously, in whole or in part, been submitted anywhere else. All the data is authentic and was developed by the authors.

Code availability The code used in this study is the open-source DEM code ESyS-Particle, available at: https://launchpad.net/esys-particle

References

Bonilla-Sierra V, Scholtès L, Donzé FV, Elmouttie M (2015) Rock slope stability analysis using photogrammetric data and DFN–DEM modelling. Acta Geotech 10:497–511

Chen X, Cui P, You Y, Chen J, Li D (2015) Engineering measures for debris flow hazard mitigation in the Wenchuan earthquake area. Eng Geol 194:73–85

Choi CE, Goodwin GR, Ng CWW, Cheung DKH, Kwan JSH, Pun WK (2016) Coarse granular flow interaction with slit structures. Géotech Lett 6:267–274

Choi S-K, Lee J-M, Kwon T-H (2018) Effect of slit-type barrier on characteristics of water-dominant debris flows: small-scale physical modeling. Landslides 15:111–122

Choi CE, Ng CWW, Law RPH, Song D, Kwan JSH, Ho KKS (2014) Computational investigation of baffle configuration on impedance of channelized debris flow. Can Geotech J 52:182–197

Choi CE, Ng CWW, Liu H, Wang Y (2019) Interaction between dry granular flow and rigid barrier with basal clearance: analytical and physical modelling. Can Geotech J 57:236–245

Crosta GB, Imposimato S, Roddeman D (2009) Numerical modeling of 2-D granular step collapse on erodible and nonerodible surface. J Geophys Res Earth Surf 114:1–19

Cucchiaro S, Cazorzi F, Marchi L, Crema S, Beinat A, Cavalli M (2019) Multi-temporal analysis of the role of check dams in a debris-flow channel: linking structural and functional connectivity. Geomorphology 345:106844

Cui Y, Choi CE, Liu LHD, Ng CWW (2018) Effects of particle size of mono-disperse granular flows impacting a rigid barrier. Nat Hazards 91:1179–1201

Dong K, Wang C, Yu A (2015) A novel method based on orientation discretization for discrete element modeling of non-spherical particles. Chem Eng Sci 126:500–516

Ferellec J, McDowell G (2010) Modelling realistic shape and particle inertia in DEM. Géotechnique 60:227–232

Goodwin GR, Choi CE (2020) Slit structures: fundamental mechanisms of mechanical trapping of granular flows. Comput Geotech 119:103376

Guises R, Xiang J, Latham J-P, Munjiza A (2009) Granular packing: numerical simulation and the characterisation of the effect of particle shape. Granul Matter 11:281–292

Hamilton WR (1844) On quaternions; or on a new system of imaginaries in algebra. London, Edinb Dublin Philos Mag J Sci 25:10–13

Han W, Ou G (2006) Efficiency of slit dam prevention against non-viscous debris flow. Wuhan Univ J Nat Sci 11:865–869

Hürlimann M, Copons R, Altimir J (2006) Detailed debris flow hazard assessment in Andorra: a multidisciplinary approach. Geomorphology 78:359–372

Ikeya H, Uehara S (1980) Experimental study about the sediment control of slit Sabo dams. Sabo Gakkaishi 32:37–44

Iverson RM (1997) The physics of debris flows. Rev Geophys 35:245–296

Iverson RM (2015) Scaling and design of landslide and debris-flow experiments. Geomorphology 244:9–20

Kwan JSH, Koo RCH, Ng CWW (2015) Landslide mobility analysis for design of multiple debris-resisting barriers. Can Geotech J 52:1345–1359

Law RPH, Choi CE, Ng CWW (2015) Discrete-element investigation of influence of granular debris flow baffles on rigid barrier impact. Can Geotech J 53:179–185

Leonardi A, Goodwin GR, Pirulli M (2019) The force exerted by granular flows on slit dams. Acta Geotech 14:1949–1963

Li X, Zhao J (2018) A unified CFD-DEM approach for modeling of debris flow impacts on flexible barriers. Int J Numer Anal Methods Geomech 42:1643–1670

Lube G, Huppert HE, Sparks RS, Freundt A (2005) Collapses of two-dimensional granular columns. Phys Rev E 72:1–10

Marchelli M, Leonardi A, Pirulli M, Scavia C (2020) On the efficiency of slit-check dams in retaining granular flows. Géotechnique 70:226–237

McArdell BW, Bartelt P, Kowalski J (2007) Field observations of basal forces and fluid pore pressure in a debris flow. Geophys Res Lett 34

Ng CWW, Choi CE, Song D, Kwan JHS, Koo RCH, Shiu HYK, Ho KKS (2015) Physical modeling of baffles influence on landslide debris mobility. Landslides 12:1–18

Shen W, Zhao T, Zhao J, Dai F, Zhou GGD (2018) Quantifying the impact of dry debris flow against a rigid barrier by DEM analyses. Eng Geol 241:86–96

Shima J, Moriyama H, Kokuryo H, Ishikawa N, Mizuyama T (2016) Prevention and mitigation of debris flow hazards by using steel open-type Sabo dams. Int J Erosion Control Eng 9:135–144

Teufelsbauer H, Wang Y, Pudasaini SP, Borja RI, Wu W (2011) DEM simulation of impact force exerted by granular flow on rigid structures. Acta Geotech 6:119–133

Utili S, Zhao T, Houlsby GT (2015) 3D DEM investigation of granular column collapse: evaluation of debris motion and its destructive power. Eng Geol 186:3–16

Wang Y (2009) A new algorithm to model the dynamics of 3-D bonded rigid bodies with rotations. Acta Geotech 4:117–127

Weatherley D, Boros V, Hancock W (2011) ESyS-Particle tutorial and user's guide version 2.1. Earth Systems Science Computational Centre, The University of Queensland

Zhao T, Crosta GB, Utili S, De Blasio FV (2017) Investigation of rock fragmentation during rockfalls and rock avalanches via 3-D discrete element analyses. J Geophys Res Earth Surf 122:678–695

Zhao T, Dai F, Xu NW, Liu Y, Xu Y (2015) A composite particle model for non-spherical particles in DEM simulations. Granul Matter 17:763–774

Zhou GGD, Hu HS, Song D, Zhao T, Chen XQ (2019) Experimental study on the regulation function of slit dam against debris flows. Landslides 16:75–90

Zhou GGD, Sun QC (2013) Three-dimensional numerical study on flow regimes of dry granular flows by DEM. Powder Technol 239:115–127

S. Gong · F. Dai
State Key Laboratory of Hydraulics and Mountain River Engineering, College of Water Resource and Hydropower,
Sichuan University,
Chengdu, 610065, China

T. Zhao
Department of Civil and Environmental Engineering,
Brunel University London,
London, UB8 3PH, UK

T. Zhao (✉) · G. G. D. Zhou
Key Laboratory of Mountain Hazards and Earth Surface Process, Institute of Mountain Hazards and Environment,
Chinese Academy of Sciences & Ministry of Water Conservancy,
Chengdu, China
Email: tao.zhao@brunel.ac.uk

J. Zhao
Department of Civil and Environmental Engineering,
The Hong Kong University of Science and Technology,
Clear Water Bay, Kowloon, Hong Kong, SAR, China